BILINGUAL PUBLISHING CO.
Pioneer of Global Academics Since 1984

Journal of Atmospheric Science Research
https://ojs.bilpublishing.com/index.php/jasr

ARTICLE

Transport and Deposition of Saharan Dust Observed from Satellite Images and Ground Measurements

Habib Senghor[1,2*] Alex J. Roberts[3] Abdou L. Dieng[2] Dahirou Wane[2] Cheikh Dione[4] Mouhamed Fall[2] Abdoulahat Diop[1] Amadou T. Gaye[2] John Marsham[3]

1.Agence nationale de l'aviation civile et de la météorologie, Sénégal
2.Laboratoire de Physique de l'Atmosphère et de l'Océan Simeon-Fongang (LPAO-SF), École Supérieure Polytechnique (ESP) de l'Université Cheikh Anta Diop (UCAD), Dakar, Sénégal
3.School of Earth and Environment, University of Leeds, LS2 9JT, UK
4.African Centre of Meteorological Applications for Development (ACMAD), Niger

ARTICLE INFO

Article history
Received: 28 April 2021
Accepted: 20 May 2021
Published Online: 22 May 2021

Keywords:
Dust
Haboob
Saharan air layer

ABSTRACT

Haboob occurrence strongly impacts the annual variability of airborne desert dust in North Africa. In fact, more dust is raised from erodible surfaces in the early summer (monsoon) season when deep convective storms are common but soil moisture and vegetation cover are low. On 27 June 2018, a large dust storm is initiated over North Africa associated with an intensive westward dust transport. Far away from emission sources, dust is transported over the Atlantic for the long distance. Dust plume is emitted by a strong surface wind and further becomes a type of haboob when it merges with the southwestward deep convective system in central Mali at 0200 UTC (27 June). We use satellite observations to describe and estimate the dust mass concentration during the event. Approximately 93% of emitted dust is removed the dry deposition from the atmosphere between sources (10°N–25°N; 1°W–8°E) and the African coast (6°N–21°N; 16°W–10°W). The convective cold pool has induced large economic and healthy damages, and death of animals in the northeastern side of Senegal. ERA5 reanalysis has shown that the convective mesoscale impacts strongly the climatological location of the Saharan heat low (SHL).

1. Introduction

Northern Hemisphere has been identified in as the largest and most persistent dust source with an important contribution of the Sahara and Sahel deserts [1,2]. Almost 70% of the global dust production are emitted from Sahara desert [3]. The seasonal timescales of the dust emission and transport [4,5] are mainly lead by various meteorological mechanisms [6].

In boreal winter, from November to February [7], the dust sources are predominantly activated by the breakdown of the Low-Level-Jet (LLJ) and the effect of the latter mechanism is mainly dominated by the Bodélé Depression in Tchad which peaks during spring and particu-

**Corresponding Author:*
Habib Senghor,
Agence nationale de l'aviation civile et de la météorologie; Laboratoire de Physique de l'Atmosphère et de l'Océan Simeon-Fongang (LPAO-SF), École Supérieure Polytechnique (ESP) de l'Université Cheikh Anta Diop (UCAD), Dakar, Sénégal;
Email: habib.senghor@ucad.edu.sn

 DOI: https://doi.org/10.30564/jasr.v4i2.3165

larly in May [6,7].

In boreal summer, the dust activity becomes very intense with a peak in June in Western Africa [4]. During this period, the dust mobilization is preferentially led by the density currents associated with the deep convective systems. The density currents usually produce dust storms in the afternoons and evenings hours [6]. In fact, the mesoscale convective systems and their associated cold pools mobilized dust with a high frequency up to 50% during nighttime [8–10]. In addition, the orographic effect of the Atlas Mountains can affect the deep moist convection by blocking the advection of the systems. This can induce density currents with an evaporative cooling of cloud particles leading high surface wind speed and dust emission[11,12]. The downward mixing of the LLJ momentum to the surface causes 60% of the total dust amount in the southern of the Hoggar-Tibesti channels [13]. The LLJ activity in the Western Sahara may strongly affect dust emission in the mountain's areas (such as Adrar and Air) in addition to the downbursts from the deep moist convection. The density currents generated by the convective storms can propagate over many hundreds of kilometers from the system and cause dust emission so-called "haboob" events[14–16].

Modeling simulations have estimated the global dust emission between 500 and 4400 Tg yr^{-1} and a range between 400 and 2200 Tg yr^{-1} from North Africa [17]. Dust raised in North Africa is predominantly transported and deposited between June and August along the main dust pathway, from Sahara region to the Americas [18–20].

Atmospheric dust can reduce the visibility [21–23], affect the radiative budget by airborne particles directly and indirectly [24]. Mineral dust influences the global CO_2 cycle[25] through the biological carbon pump, precipitation and sea surface temperature [26–28]. Besides these consequences, mineral dust impacts human health [29] with a highest prevalence of respiratory infection such as asthma, bronchitis, and tuberculosis [30,31]. Dust storms which mainly occur during the monsoon season in western Sahara can also cause transport accidents for civilians and military [32].

The large haboob that occurred, from 26 to 27 June 2018 in western Sahel, is one of the most dust storms churned in west African region. It caused important damages notified in Senegal including livestock losses as well as material damages in the northern side of the country and at Blaise Diagne International Airport (AIBD). It was identified as the onset rainfall by the National Agency of the Meteorology (ANACIM). This event has caused serious environmental, social, and economic issues with a rapid increase in the purchase prices of livestock. Consequently, an adequate description of this event is essential to improve the accuracy for weather forecasting of extreme events. To address this issue, we use in-situ measurements and satellite observations to describe the synoptic situation of this case and estimate the amount of dust loading during the event. This paper is organized as follows: section 2 describes the data and methods, section 3 presents the dust event, section 4 analyzed results, and finally a conclusion is given in section 5.

2. Data description and Methods

2.1 Observational Datasets

2.1.1 Photography

Photos taken by amateurs in Mali and Senegal on 27 June 2018 Figure 1(b-c) are used to display the haboob like features of the dust storm as well as for estimating vertical extent of the leading edge of the dust plume.

2.1.2 GOES Imagery

The Geostationary Operational Environmental Satellite Program (GOES), developed by the National Aeronautics and Space Administration (NASA) and National Oceanic and Atmospheric Administration (NOAA) [33,34] is used to visualize the studied dust event. The Imager instrument consists of five spectral bands ranging from the visible to the longwave infrared channel. The spatial resolution for the visible band is 1 km while most of the infrared has a resolution of 4 km (at nadir) and the detectors are oversampled in the east-west direction [35]. Imagery is collected every 15 min to derive many operational products such as cloud products (height, properties, etc.), atmospheric motion, biomass burning, smoke, dust, and surface properties (e.g., land surface temperature) [34]. The temporal and spatial resolution of the GOES products allows for the studied dust plume to be tracked as it moves across the Atlantic giving insight into its behavior and development.

2.1.3 SEVIRI RGB Imagery

The system is also tracked by imagery derived from the Spinning Enhanced Visible and Infrared Imager (SEVIRI) on board the Meteosat Second Generation (MSG) geostationary satellite. SEVIRI imagery has 15-minute temporal resolution and 3 km for the grid spacing for 12 channels. The SEVIRI sensor could identify dust and the cloud features using respectively pink and dark colors [36].

2.1.4 NASCube Imagery

The North African Sand Storm Survey (NASCube) algorithm processes the METEOSAT (MSG2) SEVIRI

DOI: https://doi.org/10.30564/jasr.v4i2.3165

instrument level 1.5 data from EUMETSAT and provides 24 h detection and characterization of sandstorms to track their evolution over North Africa and Saudi Arabia [37]. The NASCube with the visual long-waves imagery is used for the mesoscale convective system (MCS) monitoring near the African coast and images are collected with one hour-temporal resolution.

2.1.5 AERONET

The dust plume transported over Senegal is monitored by Aerosol Robotic Network (AERONET, [38]developed to support NASA, CNES, and NASDA's Earth satellite systems under the name AERONET and expanded by national and international collaboration, is described. Recent development of weather-resistant automatic sun and sky scanning spectral radiometers enable frequent measurements of atmospheric aerosol optical properties and precipitable water at remote sites. Transmission of automatic measurements via the geostationary satellites GOES and METEOSATS' Data Collection Systems allows reception and processing in near real-time from approximately 75% of the Earth's surface and with the expected addition of GMS, the coverage will increase to 90% in 1998. NASA developed a UNIX-based near real-time processing, display and analysis system providing internet access to the emerging global database. Information on the system is available on the project homepage, http://spamer.gsfc.nasa.gov. The philosophy of an open access database, centralized processing and a user-friendly graphical interface has contributed to the growth of international cooperation for ground-based aerosol monitoring and imposes a standardization for these measurements. The system's automatic data acquisition, transmission, and processing facilitates aerosol characterization on local, regional, and global scales with applications to transport and radiation budget studies, radiative transfer-modeling and validation of satellite aerosol retrievals. This article discusses the operation and philosophy of the monitoring system, the precision and accuracy of the measuring radiometers, a brief description of the processing system, and access to the database.",”container-title”:”Remote Sensing of Environment”,”DOI”:”10.1016/S0034-4257(98) station located in Mbour (14.76°N, 17.5°W). At this station located along the route of the haboob, we use the dust properties Aerosol Optical Depth (AOD) and Ångstrom Exponent (AE) to show the changes associated with the arrival of dust.

2.1.6 MODIS

To characterize mineral dust, we use their optical and physical properties with AOD and AE which is inversely proportional to the dust size. The westward propagation of the plume is highlighted by the daily spatial distribution of the AOD from the Moderate resolution Imaging Spectroradiometer (MODIS) [39].

The dust mass is estimated from MODIS's AOD which is mainly dominated by the contribution of desert dust aerosols uplifted at the foothills of Hoggar and Adra mountains in agreement with previous scholar [40]. Dust is quantified over land following the equation taken from [19]:

$$M_{du} = 2.7A\tau_{du} \quad (g) \qquad (1)$$

Where τ_{du} is the mean dust AOD at wavelength 550 nm, A is the plume area calculated by the regression between the AOD and aerosol column concentration in Sahelo-Saharan region [19].

2.1.7 CALIOP

The advection of the dust plume is studied using the attenuated backscatter and the polarization signal from the Cloud-Aerosol LIdar with Orthogonal Polarization (CALIOP) instrument on board the Cloud-Aerosol Lidar and Infrared Pathfinder Satellite Observation (CALIPSO) satellite [41,42]. In addition to the optical and physical properties of clouds and aerosols, CALIOP provides through the volume depolarization ratio (VDR) a characterization of the aerosol types. The VDR is defined as the ratio between the perpendicular and the parallel components of the backscatter coefficient of aerosols at 532 nm. The VDR gives a quantitative discrimination of particles shape [43] and differentiates the spherical droplets (liquid) and the nospherical (solid) [44,45]. The VDR of mineral dust is expected to be relatively high and range between 0.1 to 0.4 as heighted in [19,46,47].

2.2 Model Datasets

2.2.1 HYSPLIT

The NOAA Air Resources Laboratory's (ARL) Hybrid Single-Particle Lagrangian Integrated Trajectory model (HYSPLIT) computes the air masse trajectories and transport, dispersion, and deposition [48,49]. We use NOAA HSYPLIT model to represent the 72 hour air masse backward trajectories ending in Dakar at 1800 UTC on 27 June 2018 and all trajectories end at 2000 m height (Figure 1a).

2.2.2 ERA5 Reanalysis

The ERA5 reanalysis provides an estimation of the global atmosphere, land surface and ocean waves from 1950 to present for 1 hour temporal resolution, 31 km for the horizontal grid spacing and 137 vertical levels extent from the surface up to 0.01 hPa [50(p. 5),51]. We use the ERA5

 DOI: https://doi.org/10.30564/jasr.v4i2.3165

data to track the daily advection of the SHL during the period's event based on the atmospheric thickness between two pressure levels [52]a region of high surface temperatures and low surface pressures, is a key element of the West African monsoon system. In this study, we propose a method to detect the WAHL in order to monitor its climatological seasonal displacement over West Africa during the period 1979–2001, using the European Centre for Medium-range Weather Forecast (ECMWF:

$$\Delta Z = \frac{R}{g} \int_{p2}^{p1} Td(\ln(p)) \quad (2)$$

3. Dust Event Description

A severe sandstorm is initiated on 26 June 2018 in southern Algeria, and is transported far away from North Africa on 27 June 2018. The dust is transported over the tropical North Atlantic Ocean (Figure 1a) and detected by the GOES East satellite images over Atlantic (Figure 1d). This type of dust storm has often been observed in Arabian Peninsula, in desert areas located in the southwestern of the United States of America (USA) and finally in the largest mineral dust sources in North Africa. This haboob is very thick over Mali (Figure 1b) and Senegal (Figure 1c) and is elevated at the Saharan Air Layer (SAL) pressure levels between 1.5 and 6 km [5,53]. Figure 1a shows both northwestward and southwestward transport of air masses which merge at 0200 UTC on 27 June 2018 over western Mali. This merge powered the MCS and the strong convection created a powerful haboob which impacted local the economy, people living in the region and especially the cattle-breeder. Several hundreds of livestock deaths are noted, and planes are damaged at AIBD. The event was part of very intense uplift and has contributed to a larger dust outbreak event as shown in Figure 1d.

Figure 2 shows a development of the MCSs that produced the haboobs but the atmospheric moisture tends and clouds associated with the MCS are obscuring the detection of dust outbreaks in multispectral SEVIRI images [36]. Whatever, SEVIRI can detect the amount dust loading observed in Mauritania and North Mali where the moisture is lower. The animation of the hourly SEVIRI images has shown that the dust plume is advected from the northern side of Mali at 2200 UTC (26 June) and is associated with the development of small convective systems which are also initiated in Northeast Mali at 1600 UTC (26 June) (Figure not shown) and simultaneously a big convective system is triggered in boundaries between Togo and Ghana at 1530 UTC (26 June). The MCS detected over Togo and Ghana is strongly developed and southwestward advected in the afternoon on 26 June and covered entirely Cote d'Ivoire, Burkina Faso and southwestern Mali (Figure 2c). By 0200 UTC (27 June), both systems (coming from North and South) merge, and at 1100 UTC the mesoscale convective wrapt up a large area from the southeastern of Cote d'Ivoire to the southeastern side of Mauritania (Figure 2d).

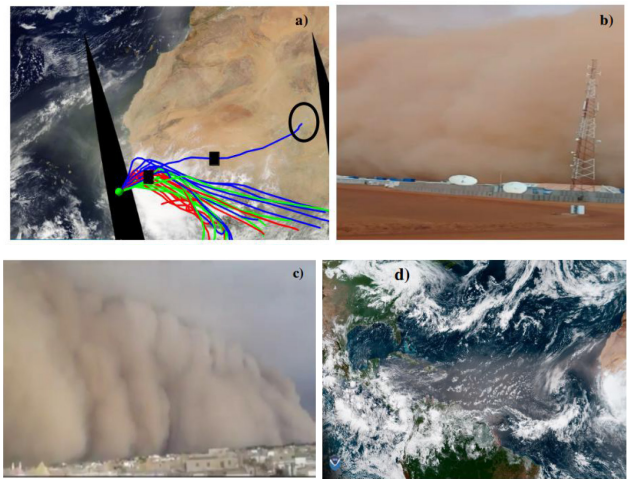

Figure 1. a) The location of the dust emission over North Africa and Westward transport indicated by the back trajectories made with the HYSPLIT model. The black regions represent the area with no satellite coverage. b) and c) are the photos taken in Mali (on 26 June) and Senegal (27 June) giving an idea of their vertical extension. The black boxes indicate the location where photos are taken. d) The dust storm traveling over the Atlantic Ocean was captured by the GOES East satellite.

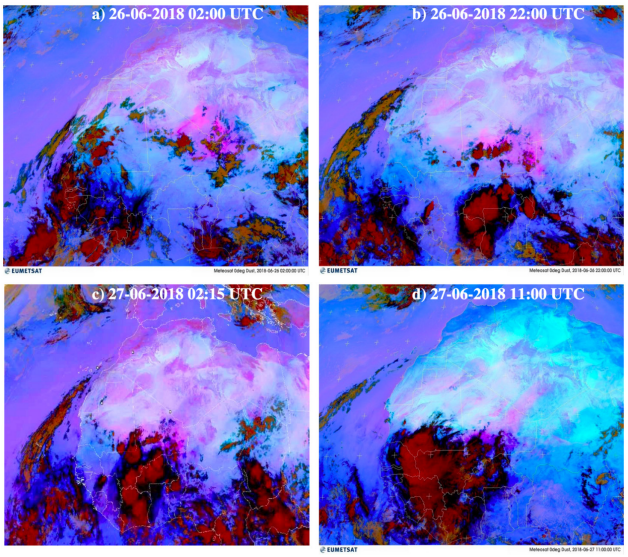

Figure 2. The SEVIRI images a) at 0200 UTC and b) 2200 UTC on 26 June, and c) 0215 UTC and d) 1100 UTC on 27 June 2018. Dark red colors represent cold cloud, bright ones show dust, which we use to track the cold pools.

DOI: https://doi.org/10.30564/jasr.v4i2.3165

Figure 3 shows the daily evolution of the SHL before and during the westward transport of the dust storm. From 24 June to 27 June 2018, a clear change is noted in the location of the SHL and a significant increase of the SHL's size is also identified (Figure 3). [52,54]a region of high surface temperatures and low surface pressures, is a key element of the West African monsoon system. In this study, we propose a method to detect the WAHL in order to monitor its climatological seasonal displacement over West Africa during the period 1979–2001, using the European Centre for Medium-range Weather Forecast (ECMWF have shown that the climatological position of the SHL is located over North Africa between Atlas and Hoggar mountains around 20–25°N during the rainy season. The cyclonic circulation in central Mali and southern side of Mauritania on 24 June induces an easterly extension of the SHL by the monsoon surge which brings moisture up to 20°N (Figure 3a). The 925 hPa geopotential shows a strong intensification of the Azores anticyclone circulation on 27 June associated with strong westward dust transport over Mauritania (Figure 3d) and northeasterly extension of the SHL in agreement with [55].

4. Results

4.1 Analysis of Aerosol Properties Using Passive Sensors

To analyze the westward transport of the dust plume, we focus on ground detection using AERONET sun-photometer in Mbour (16.95°W, 14.39°N) in Western African coast (Figure 4). The small dust particles are identified by larger AE > 0.7 and AOD < 0.5 and coarse dust particles are estimated by smaller AE < 0.7 associate to AOD > 0.5[5,56].

The daily variability of the AOD and AE shows heavy dust loading in the atmosphere from 25 to 28 June 2018. On 25 June at 1800 UTC, the atmosphere becomes slightly dusty with an increase of AOD > 0.6 and decrease of the AE < 0.1. On 26 June, the atmosphere is most clear in Mbour as shown by the low values of AOD and high values of AE in the afternoon (Figure 4). The haboob arrived to Mbour at 1300 UTC on 27 June and an abrupt change is observed on AOD which increases up to 1.9 and AE less than 0.5. Dust uplifted by the density currents and spread towards western African coast by the leading edge of the cold pool could be clearly seen in the Meteosat Second Generation (MSG) images (Figure. 6c-d).

4.2 Assessment of Dust Emissions

The spatial distribution of the hourly AOD from Nascube (Figure 5(a-b)) shows a very dusty atmosphere with AOD values greater than 1.9 over the Sahel region on 26 and 27 June. Dust emission sources can be clearly seen (Figure 5a) and the northward advection of the dust plume highlighted by maximum dust mass around 16°N and 18°N respectively on 26 and 27 June (Figure 5d). The

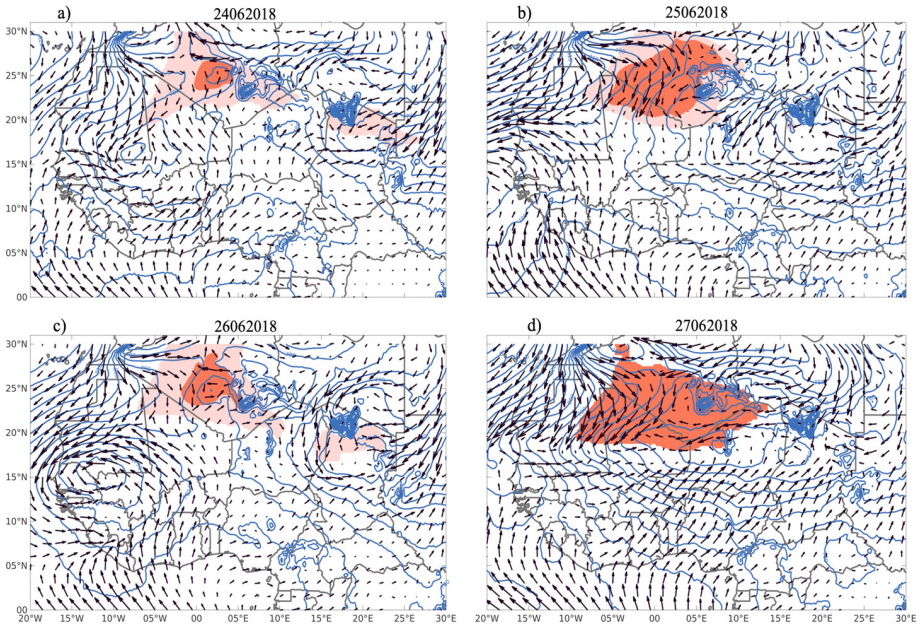

Figure 3. Color shading represent the 90 percentil of the daily mean position of the Saharan heat low and the blue lines show the 925 hPa geopotential height on: 24 June (a), 25 June b), 26 June c), and 27 June d). The 925 hPa wind vector is shown in gray arrow.

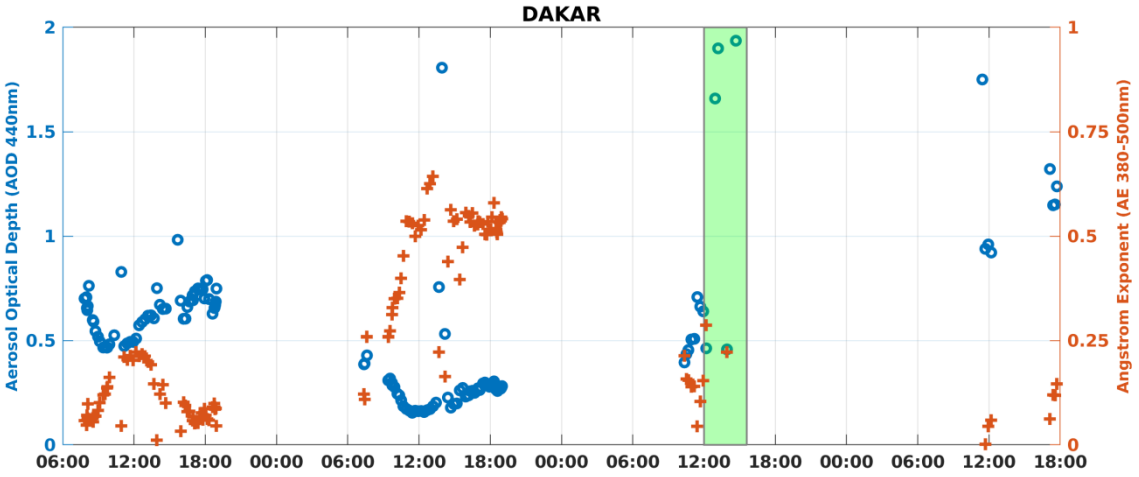

Figure 4. AOD at 400 nm and AE for 380–500 nm taken from the Aerosol Robotic Network (AERONET) at Mbour (70 km from Dakar) station from 25 to 28 June 2018. The green patch indicated the time when the dust storm overpasses towards Senegal.

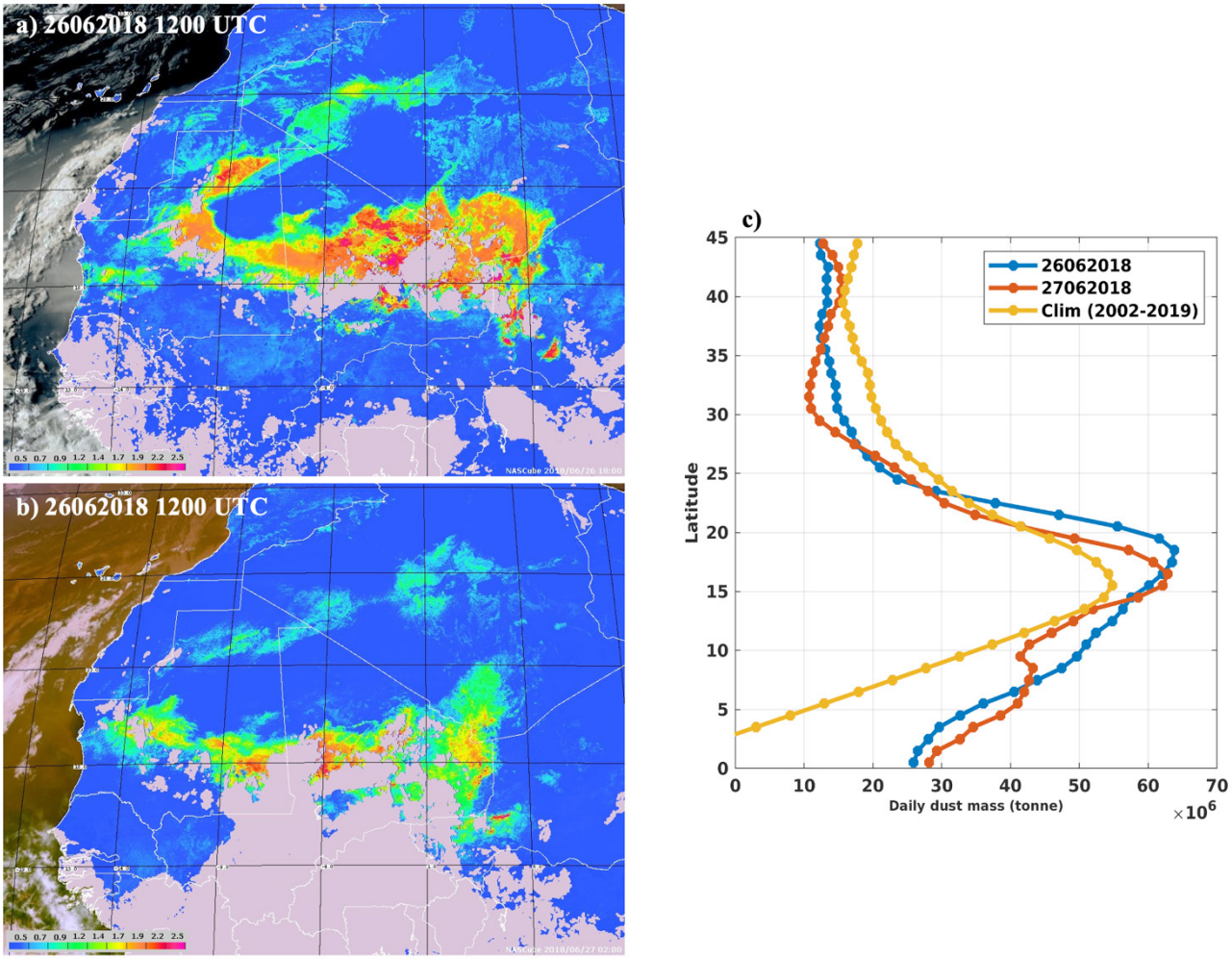

Figure 5. a) and b) respectively AOD computed from the NASCube algorithm at 1800 UTC on 26 June, and 0200 UTC on 27 June 2018. c) distribution of the dust mass estimated from the MODIS AOD and a climatological distribution between 2002 and 2019.

DOI: https://doi.org/10.30564/jasr.v4i2.3165

dust mass has shown that a significant difference is noted between 26-27 June in comparison with climatological values in the latitudinal band between 10°N and 20°N) (Figure 5d).

4.3 Vertical Distribution of the Dust Plume

As explained in term of dust mass concentration in the previous section, a clear decreasing of the dust plume thickness is shown between sources (13.13°N-25.33°N; 5.77°W-2.95°W) and African coast (13.18°N-25.38°N; 16.75°W 13.75°W), respectively on 26 June and 27 June (Figure 6a-b).

The VDR shows that the retrieved signal is mostly dominated by the dust particles with a clear indication of the dust plume transport (Figure 7c-d). Pure dust particles are given by the VDR values ranged between 0.1 and 0.4 as defined in [19]. The majority of the retrieved signals are obtained for pure dust but it is clear that the dust plume is particularly polluted by the biomass-burning indicated by VDR smaller than 0.1. The presence of clouds is shown by VDR > 0.4 (Figure 6 and Figure 7c-d).

4.4 Surface Measurements

We are now focusing on the ground-based measurements to investigate the impact of the dust storm on the weather observations in Senegal. At 09 00 UTC (27 June), when the MCS is overpassing the northeastern side of Senegal at Matam (Figure 7c), a change is observed in surface wind speed (Figure 7a). The wind directions suggest the westward advection of the MCS and the arrival of

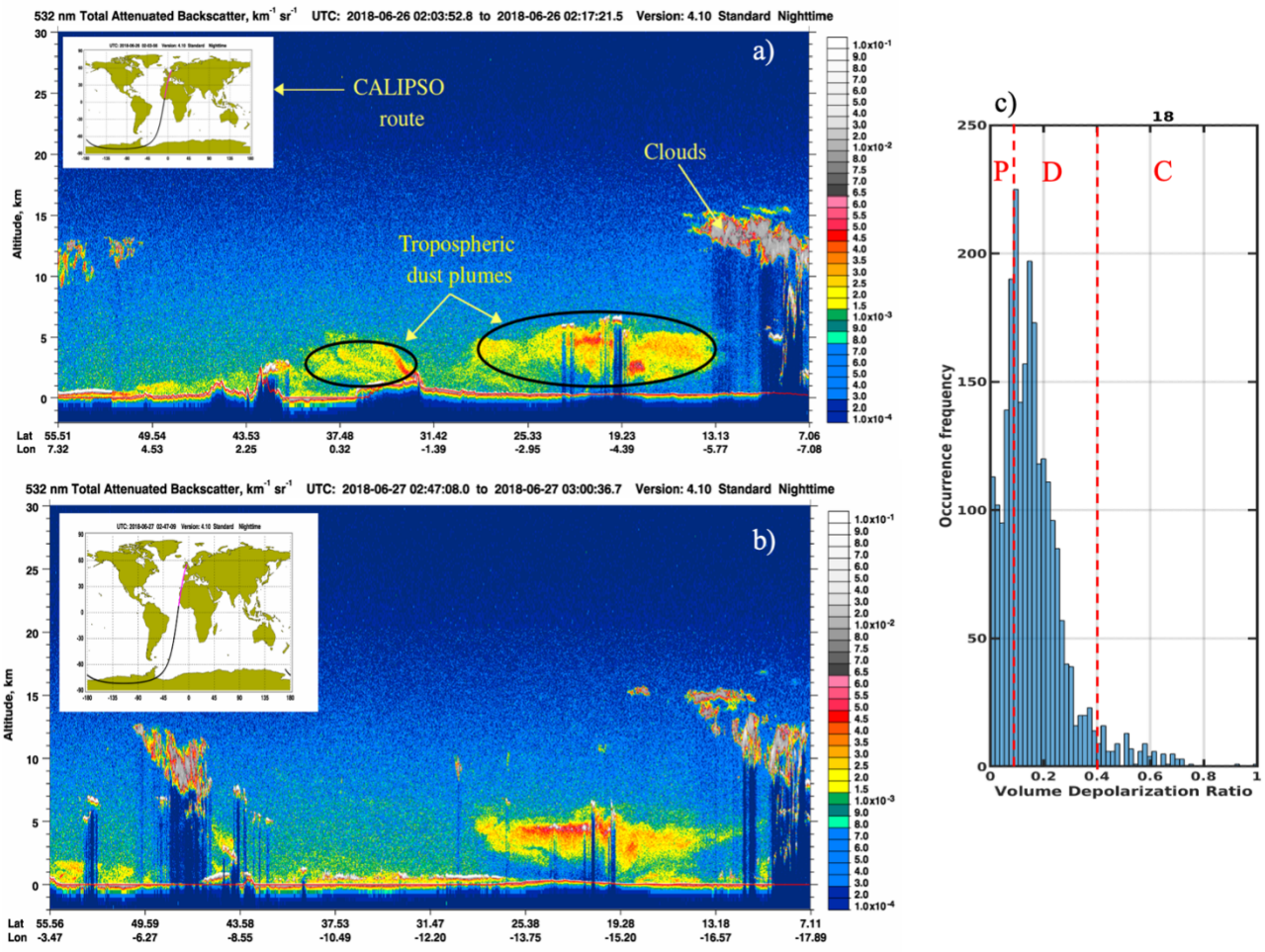

Figure 6. a) and b) CALIOP vertical attenuated backscatter profiles ($km^{-1}.sr^{-1}$) for wavelength 532nm band. The location of the dust plume, clouds and the satellite orbit are indicated in (a) at 0203 UTC on 26 June. b) shows the same characteristics with orbit in African coast. c) shows the VDR occurrence taken from the vertical cross-section covered by the aerosol plumes for the region between [13N-30N; 13W-16W] is showed by the CALIOP nighttime profiles on 27 June 2018. c) Regions dominated by pure dust (D) aerosols, clouds (C) and (P) polluted dust (mixed with biomass-burning) are respectively marked in red.

 DOI: https://doi.org/10.30564/jasr.v4i2.3165

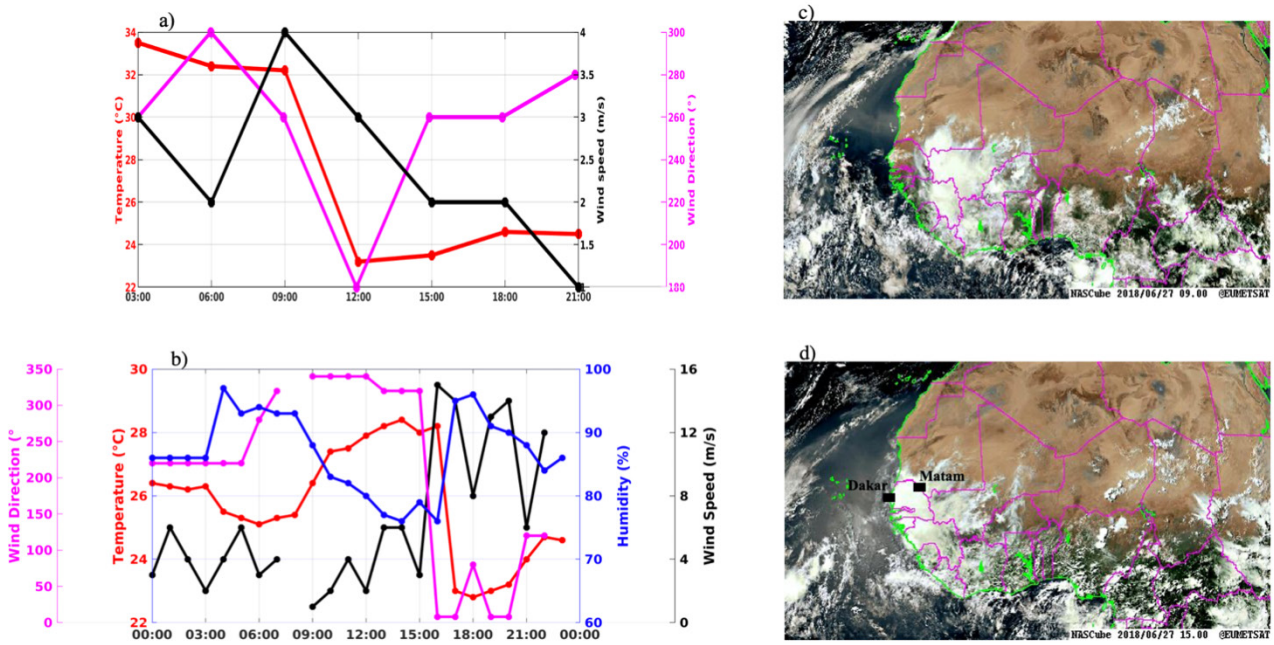

Figure 7. Surface weather variables taken from ANACIM Network stations. a) and b) Surface temperature (red lines), wind speeds (black lines), wind direction (pink lines) and the moisture (blue line), respectively at Matam (13W, 15°N) and Dakar (17°W, 14N). (c) and (d) are the Nascube images taken respectively at 0900 UTC and 1500 UTC in West Africa. Clouds are represented in white color, land in brown and surface ocean in black color. Black boxes show the position of the stations Matam and Dakar.

the cold pool outflows at Matam is shown by the drop of the surface temperature of about 9°C between 0900 and 1200 UTC, the change in wind direction.

The ground measurements taken from Dakar weather station indicate that the arrival of the MCS cold pool is shown by changes in wind direction and wind speed of about 15 $m.s^{-1}$ at 1500 UTC, the relative humidity jumps up to 90% and the drop of temperature is about 5°C (Figure 7b). The convective storms lead to local emission which are responsible for the high impact weather.

5. Conclusions

This study focuses on the description of the severe summer Saharan dust storm which occurred between 26 and 27 June 2018 over western Africa. SEVIRI, Nascube and GOES imagery have shown a clear dust storm spread by the dynamic of the density currents at the edge of the spectacular convective system. The power of this system is supported by the merge of both northwestward and southwestward convective systems and the moisture brought by the monsoon flux. Photos of the cold pool taken by amateurs, in Mali and Senegal and the CALIOP attenuated backscatter give an idea of the vertical extent of the dust plume (~5 km height). Dust mass concentration estimated by the MODIS observations shows an emission of huge quantities of dust over the Sahara region. The advection of dust is clearly shown by the surface wind less than 6 m/s at Matam in the southeasterly part of Senegal and the westward dust transport is amplified by the strong contribution of the local dust emission. The local dust emissions and strong wind speed shown by observations in Dakar have produced considerable damages on the planes of the transair company at Dakar Airport. The death of animals at Matam could be attributed to this very rare drastic reduction of the surface temperature by about 9°C. Due to the important effects of dust transport on the environment, human life and convection, it is necessary to describe and improve our understanding of the causes and processes driving this type of dust storm.

Acknowledgments

This work is supported by UK Research and Innovation as part of the Global Challenges Research Fund, African SWIFT programme, grant number NE/P021077/1. The Agence Nationale de l'Aviation civile et de la Météorologie (ANACIM), ICARE Data and services center, University of Lille, the National Aeronautics and Space Administration (NASA) and National Oceanic and Atmospheric

DOI: https://doi.org/10.30564/jasr.v4i2.3165

Administration (NOAA) are owed for sharing ground observations and satellite data.

References

[1] Prospero, J. M., Ginoux, P., Torres, O., Nicholson, S. E., & Gill, T. E. (2002). Environmental Characterization of Global Sources of Atmospheric Soil Dust Identified with the Nimbus 7 Total Ozone Mapping Spectrometer (toms) Absorbing Aerosol Product. Reviews of Geophysics, 40(1), 2-1-2-31. https://doi.org/10.1029/2000RG000095.

[2] Washington, R., Todd, M., Middleton, N. J., & Goudie, A. S. (2003). Dust-storm source areas determined by the total ozone monitoring spectrometer and surface observations. Annals of the Association of American Geographers, 93(2), 297-313.

[3] Engelstaedter, S., Tegen, I., & Washington, R. (2006). North African dust emissions and transport. Earth-Science Reviews, 79(1), 73-100. https://doi.org/10.1016/j.earscirev.2006.06.004.

[4] Engelstaedter, S., & Washington, R. (2007). Atmospheric controls on the annual cycle of North African dust. Journal of Geophysical Research: Atmospheres, 112(D3).

[5] Senghor, H., Machu, É., Hourdin, F., & Gaye, A. T. (2017). Seasonal cycle of desert aerosols in western Africa : Analysis of the coastal transition with passive and active sensors. Atmospheric Chemistry and Physics, 17(13), 8395-8410.

[6] Schepanski, K., Tegen, I., Todd, M., Heinold, B., Bönisch, G., Laurent, B., & Macke, A. (2009). Meteorological processes forcing Saharan dust emission inferred from MSG‐SEVIRI observations of subdaily dust source activation and numerical models. Journal of geophysical research: atmospheres, 114(D10).

[7] Senghor, H., Machu, É., Durán, L., Jenkins, G. S., & Gaye, A. T. (2020). Seasonal Behavior of Aerosol Vertical Concentration in Dakar and Role Played by the Sea-Breeze. Open Journal of Air Pollution, 9(1), 11-26. https://doi.org/10.4236/ojap.2020.91002.

[8] Marsham, J. H., Hobby, M., Allen, C. J. T., Banks, J. R., Bart, M., Brooks, B. J., Cavazos‐Guerra, C., Engelstaedter, S., Gascoyne, M., Lima, A. R., Martins, J. V., McQuaid, J. B., O'Leary, A., Ouchene, B., Ouladichir, A., Parker, D. J., Saci, A., Salah‐Ferroudj, M., Todd, M. C., & Washington, R. (2013). Meteorology and dust in the central Sahara : Observations from Fennec supersite-1 during the June 2011 Intensive Observation Period. Journal of Geophysical Research: Atmospheres, 118(10), 4069-4089. https://doi.org/10.1002/jgrd.50211.

[9] Allen, C. J., Washington, R., & Engelstaedter, S. (2013). Dust emission and transport mechanisms in the central Sahara : Fennec ground‐based observations from Bordj Badji Mokhtar, June 2011. Journal of Geophysical Research: Atmospheres, 118(12), 6212-6232.

[10] Heinold, B., Knippertz, P., Marsham, J., Fiedler, S., Dixon, N., Schepanski, K., Laurent, B., & Tegen, I. (2013). The role of deep convection and nocturnal low‐level jets for dust emission in summertime West Africa : Estimates from convection‐permitting simulations. Journal of Geophysical Research: Atmospheres, 118(10), 4385-4400.

[11] Droegemeier, K. K., & Wilhelmson, R. B. (1987). Numerical simulation of thunderstorm outflow dynamics. Part I: Outflow sensitivity experiments and turbulence dynamics. Journal of atmospheric sciences, 44(8), 1180-1210.

[12] Knippertz, P., Ansmann, A., Althausen, D., Müller, D., Tesche, M., Bierwirth, E., Dinter, T., Müller, T., Hoyningen-Huene, W. V., & Schepanski, K. (2009). Dust mobilization and transport in the northern Sahara during SAMUM 2006–a meteorological overview. Tellus B: Chemical and physical meteorology, 61(1), 12-31.

[13] Fiedler, S., Schepanski, K., Heinold, B., Knippertz, P., & Tegen, I. (2013). Climatology of nocturnal low‐level jets over North Africa and implications for modeling mineral dust emission. Journal of Geophysical Research: Atmospheres, 118(12), 6100-6121.

[14] Flamant, C., Chaboureau, J., Parker, D., Taylor, C., Cammas, J., Bock, O., Timouk, F., & Pelon, J. (2007). Airborne observations of the impact of a convective system on the planetary boundary layer thermodynamics and aerosol distribution in the inter‐tropical discontinuity region of the West African monsoon. Quarterly Journal of the Royal Meteorological Society: A journal of the atmospheric sciences, applied meteorology and physical oceanography, 133(626), 1175-1189.

[15] Karam, D. B., Flamant, C., Knippertz, P., Reitebuch, O., Pelon, J., Chong, M., & Dabas, A. (2008). Dust emissions over the Sahel associated with the West African monsoon intertropical discontinuity region : A representative case-study. Quarterly Journal of the Royal Meteorological Society, 134(632), 621-634. https://doi.org/10.1002/qj.244.

[16] Roberts, A., & Knippertz, P. (2014). The formation of a large summertime Saharan dust plume : Convective and synoptic‐scale analysis. Journal of Geophysical Research: Atmospheres, 119(4), 1766-1785.

 DOI: https://doi.org/10.30564/jasr.v4i2.3165

[17] Huneeus, N., Schulz, M., Balkanski, Y., Griesfeller, J., Prospero, J., Kinne, S., Bauer, S., Boucher, O., Chin, M., Dentener, F., Diehl, T., Easter, R., Fillmore, D., Ghan, S., Ginoux, P., Grini, A., Horowitz, L., Koch, D., Krol, M. C., … Zender, C. S. (2011). Global dust model intercomparison in AeroCom phase I. Atmospheric Chemistry and Physics, 11(15), 7781-7816. https://doi.org/10.5194/acp-11-7781-2011.

[18] Kaufman, Y. J., Koren, I., Remer, L. A., Tanré, D., Ginoux, P., & Fan, S. (2005). Dust transport and deposition observed from the Terra‐Moderate Resolution Imaging Spectroradiometer (MODIS) spacecraft over the Atlantic Ocean. Journal of Geophysical Research: Atmospheres, 110(D10). https://doi.org/10.1029/2003JD004436.

[19] Ben-Ami, Y., Koren, I., Rudich, Y., Artaxo, P., Martin, S., & Andreae, M. (2010). Transport of North African dust from the Bodélé depression to the Amazon Basin : A case study. Atmospheric Chemistry and Physics, 10(16), 7533-7544.

[20] Mortier, A., Goloub, P., Derimian, Y., Tanré, D., Podvin, T., Blarel, L., Deroo, C., Marticorena, B., Diallo, A., & Ndiaye, T. (2016). Climatology of aerosol properties and clear‐sky shortwave radiative effects using Lidar and Sun photometer observations in the Dakar site. Journal of Geophysical Research: Atmospheres, 121(11), 6489-6510.

[21] Petit, R., Legrand, M., Jankowiak, I., Molinié, J., Asselin de Beauville, C., Marion, G., & Mansot, J. (2005). Transport of Saharan dust over the Caribbean Islands : Study of an event. Journal of Geophysical Research: Atmospheres, 110(D18).

[22] Song, Z., Wang, J., & Wang, S. (2007). Quantitative classification of northeast Asian dust events. Journal of Geophysical Research: Atmospheres, 112(D4).

[23] Euphrasie-Clotilde, L., Plocoste, T., & Brute, F.-N. (2021). Particle Size Analysis of African Dust Haze over the Last 20 Years : A Focus on the Extreme Event of June 2020. Atmosphere, 12(4), 502.

[24] Sokolik, I. N., & Toon, O. B. (1996). Direct radiative forcing by anthropogenic airborne mineral aerosols. Nature, 381(6584), 681-683.

[25] Jickells, T., An, Z., Andersen, K. K., Baker, A., Bergametti, G., Brooks, N., Cao, J., Boyd, P., Duce, R., & Hunter, K. (2005). Global iron connections between desert dust, ocean biogeochemistry, and climate. science, 308(5718), 67-71.

[26] Prospero, J. M., & Lamb, P. J. (2003). African droughts and dust transport to the Caribbean : Climate change implications. Science, 302(5647), 1024-1027.

[27] Stuut, J., Mulitza, S., & Prange, M. (2008). Challenges to Understanding Past and Future Climate in Africa : MARUM Workshop : Response of North African Ecosystems to Abrupt Climate Change; Bremen, Germany, 14–16 November 2007.

[28] Maher, B., Prospero, J., Mackie, D., Gaiero, D., Hesse, P. P., & Balkanski, Y. (2010). Global connections between aeolian dust, climate and ocean biogeochemistry at the present day and at the last glacial maximum. Earth-Science Reviews, 99(1-2), 61-97.

[29] Prospero, J. M. (2006). Saharan dust impacts and climate change. Oceanography, 19(2), 60.

[30] Small, I., Van der Meer, J., & Upshur, R. (2001). Acting on an environmental health disaster : The case of the Aral Sea. Environmental Health Perspectives, 109(6), 547-549.

[31] Toure, N. O., Gueye, N. R. D., Mbow‐Diokhane, A., Jenkins, G. S., Li, M., Drame, M. S., Coker, K. A. R., & Thiam, K. (2019). Observed and modeled seasonal air quality and respiratory health in Senegal during 2015 and 2016. GeoHealth, 3(12), 423-442.

[32] Taheri, F., Forouzani, M., Yazdanpanah, M., & Ajili, A. (2020). How farmers perceive the impact of dust phenomenon on agricultural production activities : A Q-methodology study. Journal of Arid Environments, 173, 104028.

[33] Daniels, J. M., Gray, G., Wade, G., Schmit, T., Nelson III, J., Schreiner, A., & Holland, C. (2006). GOES sounder single field of view products. 4.

[34] Schmit, T. J., Goodman, S. J., Lindsey, D. T., Rabin, R. M., Bedka, K. M., Gunshor, M. M., Cintineo, J. L., Velden, C. S., Bachmeier, A. S., & Lindstrom, S. S. (2013). Geostationary Operational Environmental Satellite (GOES)-14 super rapid scan operations to prepare for GOES-R. Journal of Applied Remote Sensing, 7(1), 073462.

[35] Menzel, W. P., & Purdom, J. F. (1994). Introducing GOES-I: The first of a new generation of geostationary operational environmental satellites. Bulletin of the American Meteorological Society, 75(5), 757-782.

[36] Brindley, H., Knippertz, P., Ryder, C., & Ashpole, I. (2012). A critical evaluation of the ability of SEVIRI thermal IR RGB rendering to identify dust events. Part A: Theoretical analysis. J. Geophys. Res, 117, D07201.

[37] Gonzalez, L., & Briottet, X. (2017). North Africa and Saudi Arabia day/night sandstorm survey (NASCube). Remote Sensing, 9(9), 896.

[38] Holben, B. N., Eck, T. F., Slutsker, I., Tanré, D., Buis, J. P., Setzer, A., Vermote, E., Reagan, J. A., Kaufman, Y. J., Nakajima, T., Lavenu, F., Jankowiak, I., & Smirnov, A. (1998). AERONET—A

  DOI: https://doi.org/10.30564/jasr.v4i2.3165

Federated Instrument Network and Data Archive for Aerosol Characterization. Remote Sensing of Environment, 66(1), 1-16. https://doi.org/10.1016/S0034-4257(98)00031-5.

[39] Chu, D., Kaufman, Y., Ichoku, C., Remer, L., Tanré, D., & Holben, B. (2002). Validation of MODIS aerosol optical depth retrieval over land. Geophysical research letters, 29(12), MOD2-1.

[40] Weinzierl, B., Ansmann, A., Prospero, J. M., Althausen, D., Benker, N., Chouza, F., Dollner, M., Farrell, D., Fomba, W. K., Freudenthaler, V., Gasteiger, J., Groß, S., Haarig, M., Heinold, B., Kandler, K., Kristensen, T. B., Mayol-Bracero, O. L., Müller, T., Reitebuch, O., … Walser, A. (2017). The Saharan Aerosol Long-Range Transport and Aerosol–Cloud-Interaction Experiment : Overview and Selected Highlights. Bulletin of the American Meteorological Society, 98(7), 1427-1451. https://doi.org/10.1175/BAMS-D-15-00142.1.

[41] Winker, D. M. (2003). Accounting for multiple scattering in retrievals from space lidar. 5059, 128-139.

[42] Thomason, L. W., Pitts, M. C., & Winker, D. M. (2007). CALIPSO observations of stratospheric aerosols : A preliminary assessment. Atmospheric Chemistry and Physics, 7(20), 5283-5290.

[43] Noel, V., Chepfer, H., Ledanois, G., Delaval, A., & Flamant, P. H. (2002). Classification of particle effective shape ratios in cirrus clouds based on the lidar depolarization ratio. Applied optics, 41(21), 4245-4257.

[44] Sassen, K. (1991). The polarization lidar technique for cloud research : A review and current assessment. Bulletin of the American Meteorological Society, 72(12), 1848-1866.

[45] Dubovik, O., Smirnov, A., Holben, B., King, M., Kaufman, Y., Eck, T., & Slutsker, I. (2000). Accuracy assessments of aerosol optical properties retrieved from Aerosol Robotic Network (AERONET) Sun and sky radiance measurements. Journal of Geophysical Research: Atmospheres, 105(D8), 9791-9806.

[46] Murayama, T., Sugimoto, N., Uno, I., Kinoshita, K., Aoki, K., Hagiwara, N., Liu, Z., Matsui, I., Sakai, T., & Shibata, T. (2001). Ground‐based network observation of Asian dust events of April 1998 in east Asia. Journal of Geophysical Research: Atmospheres, 106(D16), 18345-18359.

[47] Liu, D., Wang, Z., Liu, Z., Winker, D., & Trepte, C. (2008). A height resolved global view of dust aerosols from the first year CALIPSO lidar measurements. Journal of Geophysical Research: Atmospheres, 113(D16).

[48] Draxler, R. R., & Hess, G. (1998). An overview of the HYSPLIT_4 modelling system for trajectories. Australian meteorological magazine, 47(4), 295-308.

[49] Stein, A., Draxler, R. R., Rolph, G. D., Stunder, B. J., Cohen, M., & Ngan, F. (2015). NOAA's HYSPLIT atmospheric transport and dispersion modeling system. Bulletin of the American Meteorological Society, 96(12), 2059-2077.

[50] Hersbach, H., Bell, B., Berrisford, P., Hirahara, S., Horányi, A., Muñoz‐Sabater, J., Nicolas, J., Peubey, C., Radu, R., & Schepers, D. (2020). The ERA5 global reanalysis. Quarterly Journal of the Royal Meteorological Society, 146(730), 1999-2049.

[51] Muñoz-Sabater, J., Dutra, E., Agustí-Panareda, A., Albergel, C., Arduini, G., Balsamo, G., Boussetta, S., Choulga, M., Harrigan, S., & Hersbach, H. (2021). ERA5-Land : A state-of-the-art global reanalysis dataset for land applications. Earth System Science Data Discussions, 1-50.

[52] Lavaysse, C., Flamant, C., Janicot, S., Parker, D. J., Lafore, J.-P., Sultan, B., & Pelon, J. (2009). Seasonal evolution of the West African heat low : A climatological perspective. Climate Dynamics, 33(2), 313-330. https://doi.org/10.1007/s00382-009-0553-4.

[53] Evan, A. T., Heidinger, A. K., & Pavolonis, M. J. (2006). Development of a new over‐water Advanced Very High Resolution Radiometer dust detection algorithm. International Journal of Remote Sensing, 27(18), 3903-3924.

[54] Ramel, R., Gallée, H., & Messager, C. (2006). On the northward shift of the West African monsoon. Climate Dynamics, 26(4), 429-440.

[55] Parker, D. J., Thorncroft, C. D., Burton, R. R., & Diongue‐Niang, A. (2005). Analysis of the African easterly jet, using aircraft observations from the JET2000 experiment. Quarterly Journal of the Royal Meteorological Society: A journal of the atmospheric sciences, applied meteorology and physical oceanography, 131(608), 1461-1482.

[56] Redmond, H. E., Dial, K. D., & Thompson, J. E. (2010). Light scattering and absorption by wind blown dust : Theory, measurement, and recent data. Aeolian Research, 2(1), 5-26.

 DOI: https://doi.org/10.30564/jasr.v4i2.3165